

Analysis of the exoplanet containing system Kepler-91

E. Budding^{1,2,3,4} • Ç. Püsküllü¹ • M. D. Rhodes⁵ •
O. Demircan¹ • A. Erdem¹

Abstract We have applied the graphical user interfaced close binary system analysis program WIN-FITTER to an intensive study of Kepler-91 using all the available photometry from the NASA Exoplanet Archive (NEA) at the Caltech website:

<http://exoplanetarchive.ipac.caltech.edu>.

Our fitting function for the tidal distortion derives from the relevant Radau equation and includes terms up to the fifth power of the fractional radius. This results in a systematic improvement in the mass ratio estimation over that of Lillo-Box et al. (2014a) and our derived value for the mass ratio is in close agreement with that inferred from recent high-resolution spectroscopic data.

It is clear that the data analysis in terms of simply an eclipsing binary system is compromised by the presence of significant other causes of light variation, in particular non-radial pulsations. We apply a low-frequency filtering procedure to separate out some of this additional light variation. Whilst the derived eccentricity appears then reduced, an eccentric effect remains in the light curve. We consider how this may be maintained in spite of likely frictional effects operating over a long time. There are also indications that could be associated with Trojan or other period-resonant mass concentrations. Suggestions of a possible secular period variation are briefly discussed.

Keywords stars – close binary; stellar dynamics; exoplanets; light curve analysis

1 Introduction

Astrophysical aims of the *Kepler* Mission, together with practical details on its construction were set out by Borucki et al. (2003). Devore et al. (2009) provided general motivational background, noting the 400 year anniversary of Kepler’s publication of the laws of elliptical orbits and equal areas in the year of the satellite’s launch. The Ames Research Center has had a prominent role in the materialization of such purposes. A comprehensive early summary was that of Borucki et al. (2011). In mid-2013 NASA announced that two out of the original four reaction wheels used in pointing the telescope on the satellite had become inoperable and the initial objectives of the mission would be compromised as a result. However, there is, by now, a large archive of photometric data inviting continued close attention and discussion.

Rhodes & Budding (2014), giving further background information relevant also to the present paper, tested their light-curve fitting software for *Kepler* exoplanet transit light curves against results published by others. They concluded that there was a fair measure of agreement about published parameter values although significant differences were found in some cases. Many of these differences can be associated with the transition of the photometric to inferred absolute parameters. Rhodes & Budding (2014) accounted for this in terms of the high sensitivity of derived mean densities to imprecisely known, but observationally obtained, surface gravities. In the case of KOI 13.01, however, it is feasible that the differences in derived inclinations **are valid and can be associated with real short term changes due to precession** (Szabó et

E. Budding

Ç. Püsküllü

M. D. Rhodes

O. Demircan

A. Erdem

¹University of Canakkale, TR 17020, Turkey;

²Carter Observatory and

³SCPS, Victoria University of Wellington and

⁴Dept. Physics & Astronomy, UoC, New Zealand.

⁵BYU, Provo, Utah

al., 2013). KOI 377.01 (= Kepler-9) is similarly open to possible variations of empirical parameters associated with orbit complexities of this known multi-planet system. For KOI 3.01, the difference in the derived stellar relative radius (r_1) may again arise from orbital complexity (Bakos et al. 2010). The unusually high limb-darkening coefficient found for Kepler-1 has remained with further study of the data and is an issue calling for continued attention and analysis, perhaps related to other peculiarities associated with this hot jupiter (Kipping & Spiegel, 2011).

The fitting program WINKEPLER, discussed in Rhodes & Budding (2014), has since been upgraded and is now called WINFITTER. It performs optimization by a modified Marquardt-Levenberg application of a fitting function to a photometric data-set (light curve). The fitting function is based on the *Radau model* developed from Kopal’s (1959) approach to the tidal and rotational distortions (ellipticity), together with the radiative interactions (reflection), of massive and relatively close gravitating bodies. It can be downloaded from <http://home.comcast.net/~michael.rhodes/>.

The upgrade allows the user the option of regular stellar eclipsing binary light curve analysis as well as that of exoplanet light curves such as those released by the *Kepler* Mission via the Mikulski Archive for Space Telescopes (MAST).

Optimal models produced by WINFITTER correspond to the least value of χ^2 , defined as $\Sigma(l_{o,i} - l_{c,i})^2/\Delta l_i^2$ (Bevington, 1969), where $l_{o,i}$ and $l_{c,i}$ are the observed and calculated light levels at a particular phase. Δl_i is an error estimate for the measured values of $l_{o,i}$. The NASA Exoplanet Archive (NEA) lists empirical values of Δl_i for each datum, which guide the values assigned to WINFITTER. Given such starting Δl_i s, we have retained flexibility in the values to be used in the χ^2 calculation, however, as it became clear that there are sources of photometric variation other than the eclipsing binary effects and photon noise. The question of what can be regarded as random noise, from the point of view of systematic effects on the close eclipsing system model, is a matter we discuss further in Section 2.2.

The theoretical light-level l_c corresponds to the given fitting function. The central problem in the analysis of photometric data, like that discussed in the present paper, is to find the best values of the parameters of this fitting function, together with the demonstration of a formally determinate optimal set of such parameters, whilst ensuring adequacy of the underlying model to account for the observed effects. Location of a single optimum in the hyperspace formed by the unknown parameters and χ^2 is effected by the simultaneous vanishing of the χ^2 derivatives with respect to all those

sought parameters. Determinacy is checked by the χ^2 Hessian staying positive definite in the vicinity of this optimum. Adequacy of the model entails that the value of χ^2/ν , where ν is the number of degrees of freedom of the data-set, should be acceptably close to unity at the optimum. Standard tabulations of the $\chi^2(\nu)$ values at given probability levels can be used to check this. Rhodes & Budding (2014) included further discussion of this subject as well as the physical basis of the modelling (cf. also Budding & Demircan, 2007 (Ch. 9); Rhodes, 2015).

2 Kepler-91

2.1 Preliminary information

Kepler-91 (= KOI 2133.01; KIC 8219268¹) is believed to contain an unusual combination of a post-Main-Sequence star ascending the Red Giant Branch accompanied by a jupiter-sized planet heated to around 2000 K (Huber et al., 2013; Lillo-Box et al., 2014a). Planetary transits are not immediately apparent in individual long-cadence data-sets: the identification was achieved by Tenenbaum et al. (2013) after applying special periodicity-finding procedures. We used the ephemeris attributed to Tenenbaum et al. (2013), as listed in the NEA, in phasing the data and the adopted epoch and period are given in Table 1. **In doing this we have assumed that the adopted Epoch does indeed correspond to an identified transit mid-minimum.** Some tens of giant planet + giant star configurations have been found hitherto and they have attracted interest related to the theory of their origin and evolution (cf. e.g. Lin et al., 1996; Johnson et al., 2007; Nagasawa et al., 2008; Villaver & Livio, 2009).

An aspect of this subject concerns possible engulfment of a close planet as the host star expands at the end of its Main Sequence stage. That Kepler-91b² is a hot jupiter in such a situation was confirmed by Lillo-Box et al. (2014a,b), and more recently by Barclay et

¹KIC stands for Kepler Input Catalogue, KIC for Kepler Object of Interest. The webpage <http://exoplanetarchive.ipac.caltech.edu/docs/data.html?redirected> guides users to numerous data-files, including the ‘cumulative list’ that we used to obtain prior parameter estimates. The official website for *Kepler* light curves is actually https://archive.stsci.edu/kepler/downloads_options.html. However, the NASA Exoplanet site referred to above does not require file-type conversion, and has convenient normalization and useful plotting options. The same light curve data can be downloaded from either site.

²The symbol b is associated with the hot jupiter component. Kepler-91 may refer to the entire system or sometimes just the host star.

al. (2015), though that picture had been contested by Esteves et al. (2013), and subsequently by Sliski & Kipping (2014). More recently, Esteves et al. (2015) have analysed a larger data-set and retracted from their previous findings. Their latest results are included in Table 4 for comparison. Some of the earlier discussion related to density estimates, whose sensitivity to error may be associated with the cubed parameter r_1 in the denominator of the constraint $\rho_\star = 3/4\pi GP^2 r_1^3$. If an absolute radius R_\star is estimated from separate evidence, the density is alternatively constrained by $\rho_\star = 3g/4\pi GR_\star$, but again a relatively large proportional error in the observationally determined value of the surface gravity g would compromise the density estimate (Muirhead et al., 2012; Rhodes & Budding, 2014).

Lillo-Box et al. (2014a), using the 2.2 m telescope at Calar Alto (Spain), checked for the possibility of background contamination associated with the relatively large angular size of the *Kepler* pixels (~ 4 arcsec). They also looked for possible non-planet-related trends in individual data segments. Commonly used flux measures have been tabulated by the archive data-source under the heading PDCSAP (pre-search data conditioning simple aperture photometry) fluxes. These data have resulted from additional processing after the SAP data (also tabulated), with the aim of mitigating data artefacts. Sometimes, investigators apply separate correction procedures on the SAP data, but Lillo-Box et al. (2014a) deemed it sufficient to utilize the listed PDCSAP information. Barclay et al. (2015) also started with the PDCSAP fluxes, though they subsequently modelled and separated out systematic effects in the data.

In preparing their analysis of the system, Lillo-Box et al. (2014a) noted the importance of reliable host star parameters, particularly where these can be elucidated by separate means prior to study of the *Kepler* photometry. They made use of high resolution spectroscopy of Kepler-91 from Calar Alto to this end, fitting, for example, model spectral energy distributions, matching individual spectral lines and including detailed asteroseismological analysis. In this way, they were able to give estimates of the radius and mass values as $6.3 \pm 0.16 R_\odot$ and $1.31 \pm 0.10 M_\odot$. Other relevant physical attributes were given too, including an age, estimated to be not far from 5 Gy, though with a substantial margin of error. Table 2 of Lillo-Box et al. (2014a) collects together stellar parameters from a variety of previous sources, where a fairly wide range of values can be noted (appreciably larger than the quoted errors). Our Table 1 assembles input information needed to build up a more comprehensive picture of the system.

The fact of pulsational activity in this star, relating to the aforementioned asteroseismological work, could

be anticipated on the basis of the arguments used in Rhodes & Budding (2014) concerning the level of scatter observed around the mean value of the stellar flux. Rhodes & Budding (2014) found that for a steady source affected only by Poissonian noise, this should work out at $\sim \psi/23.8$, where the Poisson factor $\psi = 1/\sqrt{N_f}$, N_f being the mean PDCSAP flux count, in this case for the long cadence data-sets. This would lead to a datum probable error of about 0.00012 (120 ppm), whereas what is found in typical light curve fitting is a scatter (regarded as noise) of about 3 times this level. There are thus clear indications in these data-sets of effects that regular eclipsing binary modelling does not take into account. The analysis of Barclay et al. (2015) addressed this point in some detail, though their light-curve rectification to an eclipsing binary model was on an essentially empirical basis.

2.2 *Kepler* photometry analysis

2.2.1 Preparation

In our analysis of this system using WINFITTER, we used all available long cadence data sets for the observing runs (quarters) 1-17, which we downloaded from the NEA. For each data-set we processed the listed data points using the period of Tenenbaum et al. (2013) and normalized the PDCSAP fluxes to unity. The given times of observation (BKJD) were then converted to phases in the range 0.0 to 1.0. In this way, we constructed working light curves of ~ 4000 points. These data-sets proved informative, although they appear very scattered to the eye.

For initial values of the input parameters, we could use information from the KOI (Kepler Object of Interest: cumulative list) given in the NEA (see also Batalha et al., 2013). We also take into account the parameters listed by Lillo-Box et al. (2014a), whose emphasis on prior host-star data was mentioned above (see also Seager & Mallén-Ornelas, 2003). Our Table 1 numbers are thus rounded averages from these sources. A more detailed discussion about prior possibilities for such input information was given by Barclay et al. (2015), whose analysis procedure allows for variation of hyperparameters. However, the main parameters connecting with photometric effects, such as the eclipse and its shape, constitute separate information to absolute parameter specification. Fittings to the transit minima led to reasonably consistent indications about r_1 , k and i (the radius of the star expressed as a fraction of the semi-major axis of the orbit, the ratio of planet to stellar radii, and the orbital inclination) independently of much of the information set out in Table 1. The inclination turns out to be relatively low ($\sim 70^\circ$ in Table 2) and the star is a relatively large fraction (~ 0.4 , Table 2) of the planet-star separation, so that a noticeable boundary correction (cf. Kopal, 1959; ch. 4) can occur for moderate

levels of distortion. This can delay the onset of the transit by a degree or two of phase from what would correspond to a circular stellar disk. The oft-cited formulae of Mandel and Agol (2002), used in transit analyses such as those mentioned above, could thus render the fitting function less than adequate for precise data, regardless of the precision of available priors.

Our general procedure is to approach the optimal photometric parameter specification in steps. First we concentrate on the parameters that have a relatively strong effect or are highly constrained by the light curve’s form. When these settle towards well-defined numbers, we allow for simultaneous improvements in weaker parameters. In preliminary fittings we would generally start by optimizing the scaling constant for the light curve’s vertical axis (unit of light) U ,³ and similarly the x -axis zero point (epoch of eclipse mid-minimum), or correction to the assigned phases $\Delta\phi_0$. We then use such values in subsequent runs, keeping the generally independent $\Delta\phi_0$ fixed, and optimizing for U , r_1 , k ; and i .

In Figure 1 we show our optimal fitting to the transit region. We extracted the transit portions of the light curves corresponding to the phase range -0.05 to 0.05 . Figure 1 shows the result of combining all the transit regions of all 17 light curves into a single sorted data-set of 6322 points, which has been then binned to a representative 97 points in bins of phase interval 0.001. Lillo-Box et al. (2014a) report a procedure of initial transit analysis: their Fig 6 may be compared with our Fig 1.

2.2.2 More detailed examination

Using the averaged values for the main geometric quantities from the initial fittings (bottom row of Table 2), we proceeded to examine the complete light curves. It can be readily expected from the preliminary information that proximity effects due to the relatively low separation of this hot jupiter should be detectable, although the system is fairly faint ($V = 12.884$, Everett et al., 2012) and the scatter of the data points relatively high, as noted above. In subsequent fittings to complete light curves we experimented by concentrating all the determinability of the data to optimizing

only U and the mass-ratio, q , the other parameters having been fixed from previous fittings. This procedure is sometimes called a photometric q -search. The essential form of the fitting function used here is as given in Eqn (9.17) in Budding & Demircan (2007), with further details being given in the bibliographical notes (9.7) of that book. WINFITTER has now multiplied the relative luminosities $L_{1,2}$ of the original formulation by ‘Doppler-beaming’ factors, as explained in the paper of Shporer et al (2012).

We continued with further fittings for the 17 light-curves folded over each quarter, allowing the geometric parameters to relax from previously found values. Table 2 summarizes the findings of a large number of fitting experiments as performed by our team-members separately. The run of values through the tables allows an insight into the determinability of the parameters, apart from the formal errors of each fitting. The 17th data set contains only about 1/4 of typical quarters and its best-fitting values diverged somewhat from the trend of the other solutions, while the reduced χ^2 remained relatively high. We have therefore included the results from that fitting in the tabulated mean values with a correspondingly reduced weight. At this point, we had failed to confirm any eccentricity to the orbit from these separate raw data-sets through finding a significant improvement in χ^2 from inclusion of optimized e and ω values.

We also looked for any trend that might be discernible in the values of $\Delta\phi_0$, which relates to the time of transit variation (TTV) exhibited in some exoplanet systems. Our results on this are indicated in Figure 2 with the corresponding numbers in column 3 of Table 2⁴. The inclusion of a linear correlation (incorrectly assigned period) improves the value of χ^2 , but only marginally, and, in fact, χ^2/ν is not significantly altered. A more noticeable reduction in χ^2/ν (19%) is obtained by the parabolic fit (decreasing period) but the decrease is from around a one in three ratio of exceeding the higher χ^2/ν by pure chance, to around a one in three ratio of being less than the lower χ^2/ν value randomly, and so cannot be considered significant. Alternatively, the Bayesian information criterion (BIC), which is easily related to the χ^2 variate using the formula of Kass & Raftery (1995), gives a very small preference for simply keeping the adopted period with a slight change of the reference epoch. But the first 3 fittings (reference point only, linear, and parabolic trends, have no significant difference in corresponding

³In principle, the adopted value of U could be used to scale the representative flux from the system and thence derive a corresponding stellar magnitude. However, probably related to the wide passband of the *Kepler* filter, the calibration in question turns out not simple, and we can see an appreciable departure from the trend of magnitudes with effective wavelength listed in Table 3 of Lillo-Box et al (2014a) in the case of the *Kepler* magnitude. Our flux-derived *Kepler* magnitude (12.408) thus appears too faint at the flux-weighted wavelength $0.735 \mu\text{m}$, as judged by the run of values cited by Lillo-Box et al. (2014a).

⁴It should be noted that the effects shown in Fig. 2 are not timing variations of individual transits, but an average result for each quarter. Any trend that might be discerned would not be commensurate with the orbital period therefore.

BIC values (23.3, 25.0, 24.2; respectively), though a 4-parameter fit (BIC = 27.0) would not be supported, by the assessment table of Kass & Raftery.

In fact, the implications of such a period reduction would be the highly unexpected circumstance of catching a planet within a few thousand of years before its demise. On the contrary, Sato et al (2015) gave a slightly increased period value from that given by Tenenbaum et al. (2013) (see Table 4). There are, however, interesting alternative physical scenarios relating to period changes that we discuss later.

We next combined all ~ 65000 data points into a representative binned light curve that we fitted in various ways, starting by using the mean parameters given at the bottom of Table 2. The results are summarized in Table 3. We can note here the good measure of agreement on the main geometric parameters (r_1 , k and i), as well as the mass ratio, from the various fitting approaches.

Lillo-Box et al. (2014a) carried out a basically similar procedure, aiming also to determine a planet to star mass ratio, and thence, using their separate information on the star, a planetary mass. Their fitting function combines the three contributions of ellipticity, Doppler beaming (a relatively very small term) and reflection, given by their Eqns 7, 8 & 9, respectively. Eqns 7 and 9 are very simple, however, and although their key ellipticity contribution derives originally from the same Radau-model formulae that we use (Kopal, 1959), the neglect of the third and fourth order terms in the tidal distortion (given the large relative size of the star) turns out to lead to a significant overestimate of the mass ratio as determined from the photometric effect of the stellar tide. Given that $r_1 \approx 0.4$ we can see that the neglect of the third and fourth order terms will bring their mass ratio (0.00064) down to a value in close agreement with ours.

Lillo-Box et al. (2014a) gave the planet's mass to be about $0.88 + 0.17 / - 0.33 M_{\text{Jup}}$ but with radius about $1.384 + 0.11 / - 0.054 R_{\text{Jup}}$, i.e. a density of about 1/3 that of Jupiter. This was interpreted as an atmospheric inflation, associated with the relatively high stellar irradiation. They also reported an eccentric orbit ($e = 0.066 + 0.013 / - 0.017$, $\omega = 316.8 + 21 / - 7.4$ deg), associated primarily with an apparent asymmetry of the light curve as a whole. They could not confirm this definitely from asymmetry of the transit alone, accepting that the eclipse effect was inconclusive regarding eccentricity. Our findings are similar on this point (Table 3). The complete light curve they modelled consists of about 260 individual points that have been binned from the original complete data-set, from which they

had clipped outliers so as to arrive at a working sample of ~ 52000 points. From our fittings to the original data-sets we estimated the s.d. scatter of such data at ~ 0.00037 , hence the error-bars shown on the light curve of Lillo-Box et al. (2014a) should be typically around 0.00002 on a Poissonian assumption of their distribution. This corresponds to the error bars shown in their Fig 7.

It is clear from that Fig 7, however, that the residuals are not distributed randomly around the model curve with this precision. The model curve goes through quite fewer than $\sim 2/3$ of the shown error bars, that one could reasonably expect it would do on the basis that the data corresponds only to the close binary model plus random noise. But this would happen anyway as a result of the pulsational effects. This matter was addressed by Barclay et al. (2015), who introduced an additional empirical noise model that they attributed to the effects of surface granulation of the host star. We digitized the data points of Fig 7 in Lillo-Box et al. (2014a) and could mostly confirm their model parameters to within reasonable errors including a similar eccentricity result. In order to probe the situation further we binned the source data and applied WINFITTER to the resulting light curve.

A periodicity analysis was then carried out on the residuals from this fitting. We show the result in Figure 3 (see also the residuals in Figs 4 and 5). A very significant peak at $\sim 6/P$ frequency can be seen, with a lower but wider peak at the $3/P$ submultiple. The corresponding photometric contribution, persisting throughout the ~ 240 orbits of the complete data-set, points to an orbit-oscillation resonance. This may well correspond to the beat which is produced at $\sim 11.0 \mu\text{Hz}$ between the higher frequency L2 and L0 modes shown by Lillo-Box et al (2014a), particularly the strong ones (n9L02 and n11L00) between ~ 104 and $115 \mu\text{Hz}$. The existence of this additional photometric effect is, of course, of interest in its own right; its continuation evident in the orbitally phased and binned light curve even to the eye. The nature of this resonance invites further physical discussion that we raise in Section 3. From the more immediate aim of parametrization of the close binary (star + planet) configuration, however, this is a complication that it would be desirable to separate out. Its retention in the analysis of Lillo-Box et al (2014a) may compromise the deduction of an eccentricity effect, or the parametrization in general, to some extent.

We therefore carried out a cleaning operation by fitting the residuals from the original light curve fit with a Fourier decomposition reaching to terms in frequency $6/P$. This fitting is shown in Figure 4. Our procedure is similar to that used in the cleaning of close binary systems showing maculation effects (Zeilik et al., 1988). In

Table 1 Primary Input Data

KOI	V	M_*	R_*	T_*	Epoch	P	Z	$\log g$	a	M_p/M_*	u
2133.01	12.884	1.3	6.4	4600	2454969.3966	6.246580	0.11	2.94	0.073	0.00005	0.74

We have here used the notation: V – conventional V magnitude, M_* – mass of star (solar masses), R_* – radius of star (solar radii), T_* – temperature of star (K), P – orbital period (in days), Z – metallicity of star, $\log g$ – \log_{10} of the surface gravity of star, a – semi-major axis in AUs, M_p/M_* – ratio of planet to star masses, u – stellar (linear) limb-darkening coefficient. The numbers given in this table are rounded averages from the results of Lillo-Box (2014a) and various sources provided by the NEA, including the cumulative list, the confirmed planets and exoplanet transit survey data.

Table 2 Results of optimal fittings to light curves drawn from the 17 available quarters.

Qtr	U	$\Delta\phi_0$	r_1	k	r_2	$i(\text{deg})$	q
1	1.00079	-1.5	0.404	0.0261	0.0105	68.2	0.00039
2	1.00084	-0.5	0.406	0.0247	0.0100	68.5	0.00040
3	0.99972	0.2	0.403	0.0209	0.0084	69.1	0.00037
4	0.99987	0.3	0.403	0.0206	0.0083	70.0	0.00021
5	0.99985	-0.6	0.403	0.0229	0.0092	70.1	0.00039
6	0.99991	2.0	0.407	0.0228	0.0092	68.6	0.00065
7	0.99980	0.6	0.403	0.0183	0.0074	69.8	0.00048
8	0.99981	0.6	0.400	0.0224	0.0089	70.4	0.00046
9	0.99984	-0.4	0.393	0.0215	0.0084	70.3	0.00027
10	0.99984	0.7	0.406	0.0229	0.0093	69.1	0.00051
11	0.99988	-2.1	0.405	0.0237	0.0096	68.9	0.00054
12	0.99984	0.5	0.396	0.0220	0.0087	69.5	0.00042
13	1.00000	-0.6	0.395	0.0220	0.0087	70.1	0.00012
14	1.00002	-0.9	0.403	0.0221	0.0089	69.6	0.00036
15	0.99994	0.6	0.405	0.0206	0.0084	68.8	0.00056
16	0.99967	-1.7	0.407	0.0213	0.0086	69.9	0.00048
17	0.99948	-0.5	0.409	0.0196	0.0080	69.2	0.00055
Mean	0.99999(34)	-0.2(1.0)	0.4026(43)	0.0220(18)	0.0089(7)	69.4(7)	0.00045(6)

effect, we treat the light-curve oscillatory disturbance as a low-frequency superposition. The higher frequency components that may also be present become strong at ~ 10 times our frequency limit, but such high frequency components are more akin to noise in their effects on the eclipsing binary model. Our final cleaned model and its fitting are shown in Figure 5. We may note that the cleaned light curve shows a reduced eccentricity: a direct fitting of the raw data may thus be open to doubt if interpreted simply as a real elliptical orbit. At least, its determination in a data-set containing both eclipsing binary and other causes of photometric variability cannot be taken at face value.

In Table 4 our final results and their implications for absolute parameters are listed and compared with the results of other authors.

3 Discussion

3.1 Mass ratio

The preceding presentation on the *Kepler* Mission’s photometric data on the Kepler-91 system to a large extent supports the picture given by Lillo-Box et al. (2014a, b), Barclay et al. (2015), Sato et al. (2015) and Esteves et al. (2015). The close binary system photometry analysis program WINFITTER that we have adapted and applied, however, includes a fuller description of the surface distortions due to tides and rotation, as well as the reflection effect, than has generally been used in similar studies hitherto. Given the relatively large fractional size of the star in the present case the higher power terms are significant and we can expect a systematic improvement in the mass ratio (reduced by $\sim 40\%$ from that determined by Lillo-Box et al., 2014a). Our derived value $q \approx 0.00044 \pm 0.00006$ for the mass ratio is then in good agreement with that which can be inferred from the relatively high-accuracy radial velocity data of Barclay et al. (2015) and perhaps even more with the greater coverage and higher mean accuracy results of Sato et al. (2015).

3.2 Additional effects

It is clear from the comparison of the observed scatter in the data compared with the photon noise expectable for a $V \approx 12.88$ star that there are additional short term variations, which can be associated with the non-radial pulsational spectrum also studied by Lillo-Box et al (2014a). In fact, the scatter in the raw data makes individual planetary transits only 1σ events: binning by a factor of ~ 100 therefore appears desirable to allow a reasonably confident approach to parametrization. From the empirical point of view, the light curve produced in this way can be characterized by, in addition to regular eclipsing binary system effects, (a) an ‘O’Connell effect’ (asymmetric maxima) and (b) the persistence of quasi-periodic small light drops or dims. The former can be associated with the effect of orbital eccentricity, given the slight, though calculable, effects of a correspondingly varying tidal distortion of the star. The possibility of photometric effects associated with some surface maculation may be mentioned, given the cool temperature and likely structure of this star. We know, however, from the slow rotation speed derived by Lillo-Box et al (2014a) that the planet performs around 7.6 revolutions in one rotation of the star (unlike the synchronized arrangement usually found in close binary stars – cf. e.g. Zahn, 1977). Maculation seems thus unlikely to persist as coherent systematic effects in the binned light curve in general, though starspots may be partly associated with the relatively high scatter.

Table 3 Results of optimal fittings to various light curve data-sets.

	$\Delta\phi_0$	r_1 E1	k E2	r_2 E3	i (deg)	q E4	e	ω	χ^2/ν	Δl E5
TO	-0.15(4)	4.08(7)	2.21(3)	8.9(2)	68.9(5)					
BF	-0.2(3)	4.03(6)	2.16(2)	8.7(2)	69.6(5)	4.2(8)			1.19	2.5
BFe	-0.3(2)	4.09(4)	2.22(2)	9.04(8)	69.8(4)	4.4(6)	0.05(2)	300(15)	1.07	2.5
BTO	-0.1(1)	4.1 (2)	2.2(1)	8.9(4)	68.7(8)	7(7)			1.01	2.2
BTOe	-0.1	4.1	2.1	8.8	69	6	0.03	260	1.01	2.2
NEAK		3.8(2)	2.159(+8,-31)	8.2	71.05					
NEAC					67.4(6)	4.8(6)				
LB		4.08(+1,-2)	2.26(+3,-10)		69(1)	6.4(+1,-2)				

Table 3 notation

TO = Transit Only: means from the individual runs of each quarter
 BF = Binned Full: fitting to a single binning down to 360 points
 BFe = Binned Full: as above, but with eccentricity allowed
 BTO = Binned Transit Only: fitting of all transits, binned to 256 points
 BTOe = Binned Transit Only: as above, but with eccentricity allowed
 NEAK = NASA Exoplanet Archive KOI Cumulative list
 NEAC = NASA Exoplanet Archive - Confirmed Planets
 LB = Lillo-Box et al., (2013)

Formal error estimates, where available, are indicated by the digits in parentheses. For reasons of space and convenient comparison in one panel, these are here truncated to the rightmost digits in the parameter values. En means that the listed value is 10^n times the actual value. The unit of light values (U) for these fittings (not given here) are close to unity, with the very low scatter consistent with the errors indicated in Table 3 (i.e. ~ 23 ppm for Δl or ~ 1 ppm for ΔU).

The BFe row of this table is adopted for our final presentation in Table 4. We present the reduced χ^2/ν value for this and the BF solution with the same error estimate of 0.000025 for the normalized 360 point binned data-set. The decrease of χ^2/ν from 1.19 to 1.07 is significant at the 95% confidence level, i.e. there is a relatively high probability to to the improvement produced by an eccentric orbit model. This is not the case for the transit-only fittings, where, though modelling is effective in reducing the relative scatter of the residuals, the parameters are less well defined. In fact, if eccentricity is allowed to be simultaneously adjustable the χ^2 Hessian becomes non-positive-definite, so that regular error estimates lose meaning.

Table 4 We list here the Lillo-Box et al. (2014a) (LB) parameters, as well as those of Barclay et al. (2015), Sato et al. (2015) and Esteves et al. (2015), alongside those of the present paper (P). Error estimates, influenced by the compilation of results, are listed in the final column. Where no error is listed the corresponding parameter has been taken from information separate to the fitting.

Parameter	LB	Barclay	Sato	Esteves	P	Error
Epoch	2454969.3966	2454969.3837	2454969.3866	2454969.3958	—	
P (d)	6.24658		6.24668005	6.24658	—	
dist. (pc)	1030				—	
M_s (\odot)	1.31	1.31	1.31	1.31	1.3	
T_p (K)	2000		1920 - 2460	2040 - 3000	2000	
a (\odot)	15.62	15.53	15.93	15.71	15.57	
$\log g_s$	2.95			2.953	2.96	
M_p/M_s	0.00061	0.00053	0.00048	0.00059	0.00044	0.00006
r_s (mean)	0.403	0.406	0.406	0.401	0.409	0.004
r_p (mean)	0.0091	0.0088	0.0090	0.0087	0.0090	0.0002
i (deg)	67-78	69.17	67.37	69.7	69.8	0.5
e	0.07	0.02	0.04	0.0	0.05	0.02
ω (deg)	320.0	41.9	302.8		300	20
b	0.88	0.87	0.90	0.87	0.85	0.03

In the P column — indicates values as in LB.

3.3 Explaining the dims

Regarding the dims, Lillo-Box et al. raised possible lines of explanation involving other planets or satellites that co-rotate synchronously or are in a resonant arrangement with Kepler-91b. The idea of eclipses of the planet’s reflected light, although apparently modelled by Barclay et al. (2015), faces at least conceptual difficulties, since the dims are more than twice as deep as the regular scale of reflected light at full phase. When this is eclipsed out at the secondary minimum the light level should not be appreciably lower than at phases just outside the primary minimum; the star’s light only being received in either case. We have to countenance also improbability going with the paired circumstances of another planet’s non-coplanar orbit, though still near the line of sight, which is *also* at a resonant period.

Given the v-shaped effect at phase $\sim 60^\circ$ the possibility of a large Trojan concentration can be considered: similarly, perhaps a Hilda concentration could be associated with the extra light loss about the secondary minimum. Such situations have been examined, for example by Schwarz et al. (2007), or in the volume edited by Souchay & Dvorak (2010), but more detailed clarifying explanation is needed. It seems clear that additional systematic effects are present in the light curve that survive the repeated foldings and should therefore have some connection to the orbit. However, it is also seen that the depth of the dims is $\sim 1/10$ that of the transit, entailing that any planetoid concentration must involve the equivalent of at least several thousand Vesta-sized objects if it is to fully account for the scale of light loss. The effect is several orders of magnitude greater than could apply to the Trojan concentration in the Solar System (Yoshida & Nakamura, 2005), and so must be regarded cautiously.

Lillo-Box et al. (2014a) mentioned subtle effects associated with the *Kepler* data-processing. A known effect associated with the relatively large pixel size of the *Kepler* detectors is the presence of a remote Algol system in the field. There would again be a paired coincidence required in such a case associated with the orbital period integral sub-multiplicity. Additionally, false-positive scenarios of this kind diminish to low probability following high-resolution analysis of data from the AstraLux lucky-imaging camera on the 2.2 m telescope at the Calar Alto Observatory included in the study of Lillo-Box et al. (2014a). The more direct line of interpretation raised in the previous section is thus favoured, though the suggested pipeline error possibility cannot be entirely ruled out.

Our treatment, introducing a low pass filter to remove these apparently systematic and orbitally resonant effects, leads to more precise eclipsing binary

model defined parameters, as with the approach of Barclay et al. (2015), as well as casting doubt on the precise representation of light curve asymmetry in terms of simply an elliptical orbit. Nevertheless, the light curve asymmetry is maintained even after cleaning and the most direct explanation of that is in terms of a slightly eccentric orbit, even given an expectable trend towards orbit circularization (Zahn, 1977), keeping in mind the great age of the system estimated by Lillo-Box et al. (2014a). At this point, we may note the possibility of orbital eccentricity – resonant pulsational interactions, as considered, for example, in ‘heartbeat’ pulsators (as an extreme case: see e.g. Hambleton et al., 2013). Physically, the argument is that an orbital eccentricity that might otherwise be frictionally eroded can be trapped at a certain value if appropriate amounts of energy are fed back into the orbit at just the right times from a suitable κ -mechanism (Henrard, 1982; Alexander, 1988; Witte and Savonije, 1997). However, the potentially resonant process here is actually a beat effect, rather than a direct eigenfrequency of the underlying kappa-mechanism. Even so, the amplitude envelope of selected strong eigenfunction pairs does apparently resonate at $6/P$ with the orbital frequency. That the suggested mechanism is, or is not, possible physically, thus invites fuller follow-up theoretical consideration.

3.4 Period variation

Our modelling suggested the possibility of a steady decline in the period, although the likelihood of this is not high, given the uncertainties of the time of minimum determination. On the other hand, there appears some suggestion, from the results of Sato et al. (2015) that the period may be increasing in the short term. In a similar way, an apparent trend to decrease of the longitude of periastron over the full range of the *Kepler* Mission surveillance cannot be taken so seriously given the relatively high errors of the determination.

But, in connection with such effects, Budding (1984) gave a possible form for the variation of the separation A between the components of a binary system with total mass M and two stellar masses m_1, m_2 , in which mass loss and transfer was taking place as

$$\frac{\dot{A}}{A} = 2 \left\{ \frac{\dot{J}}{J} - \frac{\dot{m}_1}{m_1} - \frac{\dot{m}_2}{m_2} - M(\dot{\epsilon}_1 + \dot{\epsilon}_2 + \dot{\epsilon}_3) \right\}, \quad (1)$$

where J is the system’s angular momentum, and the small components in ϵ_i are associated with the rotational changes of the two bodies and some surrounding matter. These latter components are often neglected, at least in a preliminary assessment.

In classical Algols, regarded as involved in a process of *mass transfer* and where m_1 denotes the originally

more massive and mass-losing star, this equation can be simplified to

$$\frac{\dot{A}}{A} \approx 2 \left\{ \frac{\dot{J}}{J} - \frac{\dot{m}_1}{m_1} \cdot \frac{(M - 2m_1)}{(M - m_1)} \right\} \quad (2)$$

where we have written simply $\dot{m}_2 = -\dot{m}_1$. In a mass loss process, \dot{m}_1 is, by definition negative, so this equation tells us that once m_1 has dropped below half the system's mass, further mass loss will widen out the separation, unless there is some significant loss of system angular momentum through \dot{J}/J . This is usually considered small for classical Algols in the process of conservative mass transfer, so the separation of the components in this phase is expected to increase. If m_1 were to become very small, but still engaging in mass transfer in this way Eqn 2 has a small denominator, which would tend to amplify the separative effect of even a low rate of mass transfer. It is feasible that the planet Kepler-91b might be losing mass in this way through the atmospheric inflation process considered by Lillo-Box et al. (2014a). The mean density of the planet certainly seems low in comparison to more typical hot jupiters. This might then be consistent with the apparent period increase indicated by Sato et al (2015).

Various possibilities that might produce a noticeable variation of \dot{J}/J could be considered, including tidal friction and magnetic braking. The latter offers a wide range of possible parameter variation and appears able to introduce significant effects in a variety of situations. In general, of course, we should expect such frictional effects to make for a negative \dot{J}/J , which would entail period decrease, as suggested in Figure 2. Reasonable estimates for \dot{J}/J due to magnetic braking were estimated by Demircan et al. (2006) and also Erdem & Öztürk (2014). However, the scale of effect that might be interpreted from Figure 2 has $\dot{P}/P \sim 10^{-7}$, which is a 2-3 orders of magnitude greater than the effects considered in these papers. Granted that the scale of error in Fig. 2 makes any present attempt at interpretation in physical terms unrealistic, still the *possibility* of period changes is intriguing. A magnetically driven mass loss, tending to decrease the orbital period, could be reasonably expected from this star; while mass transfer from the inflated planet would increase the period. The combination of effects in the Kepler-91 system overall thus make for interesting alternatives, and the case for continued surveillance is compelling.

This research has been supported by TUBITAK (Scientific and Technological Research Council of Turkey) under Grant No. 113F353. The help of colleagues in the Physics Dept., COMU, including Dr M. Tüysüz, is acknowledged.

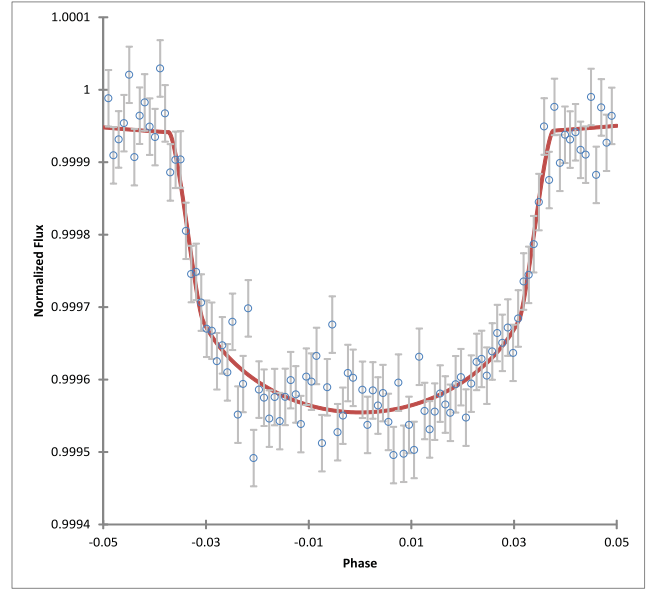


Fig. 1 Binned data covering the transit region for Kepler-91b, matched by the WINFITTER model. This may be compared with Fig. 6 in Lillo-Box et al. (2014a), or Fig. 4 in Esteves et al. (2015).

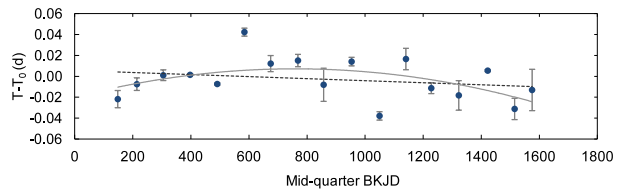


Fig. 2 Differences in observed and determined times of minimum for Kepler-91. The straight line (dashed) fit is suggestive that the assigned period may have been too long – by about 0.00001 d – but the resulting improvement is not significant. Somewhat greater significance (in a χ^2/ν sense) attaches to the secular period decrease (parabola), but even there the improvement in probability is not high (see text).

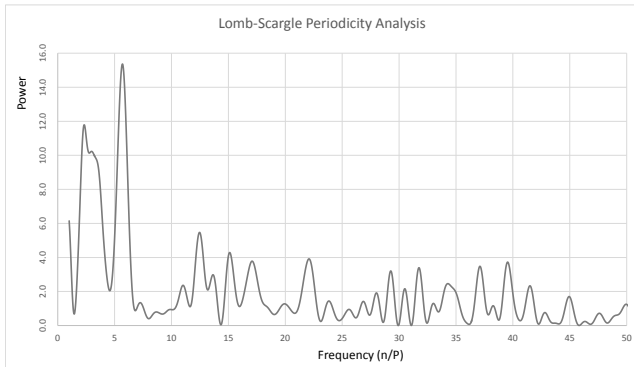


Fig. 3 Lomb-Scargle analysis of the power in the Kepler-91b light curve residuals against orbital frequency. Residuals here come from the differences between the eclipsing binary model fitting to the whole, or full-phase, data-set; originally of ~ 65000 points, but binned for this analysis to a representative 360 points. The high peak at $6/P$ is very distinct.

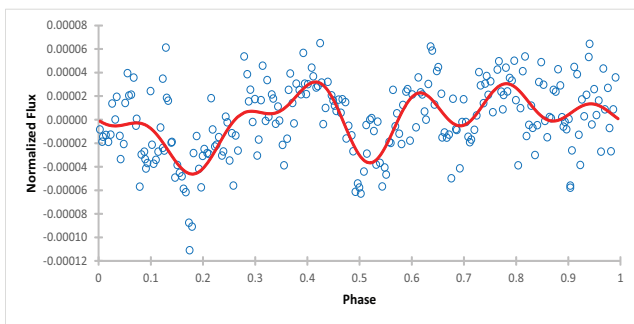


Fig. 4 Fit of a Fourier series with terms up to $6 \times$ the orbital frequency. The dips at phases $\sim 1/6$ and $\sim 1/2$ look distinct and may suggest Trojan or Hilda type phenomena. This model was added back with a negative sign to the original data-set.

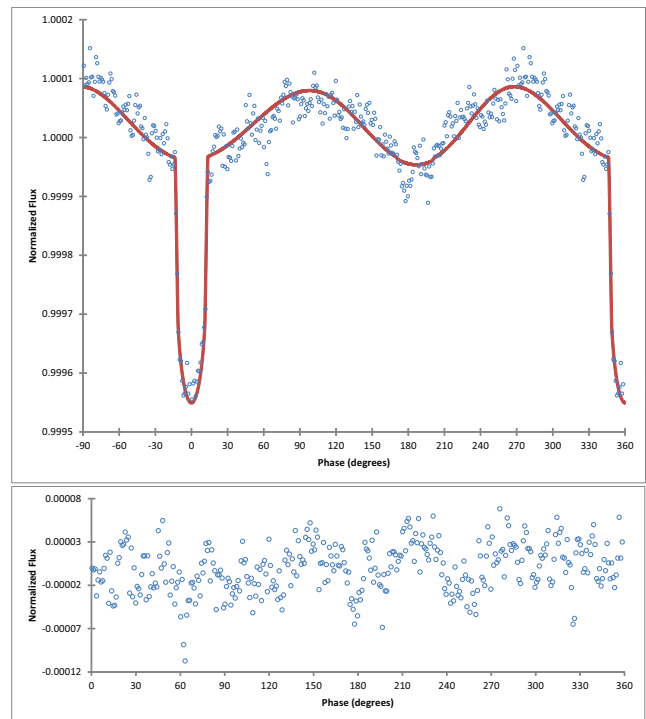


Fig. 5 Complete cleaned and binned light curve of Kepler-91, showing proximity effects and an apparent secondary minimum, together with the WINFITTER model. The residuals are shown below. This may be compared with Fig 7 in Lillo-Box et al. (2014a).

References

- Alexander M.E., 1988, MNRAS, 235, 1367
 Bakos, G.Á, et al. (24 authors), 2010, ApJ, 710, 1724
 Barclay, T., Endl, M., Huber, D., Foreman-Mackey, D., Cochran, W.D., MacQueen, P.J., Rowe, J.F., Quintana E.V., 2015, ApJ, 800, 46
 Batalha, N.M., et al. (77 authors), 2013, ApJSS, 204, 24
 Bevington, P.R., 1969, *Data Reduction and Error Analysis for the Physical Sciences*, McGraw-Hill, New York
 Borucki, W.J., et al. (13 authors), 2003, Prof. Conf. Towards Other Earths, Eds. M. Fridlung, T. Henning, ESA-SP-539
 Borucki, W.J., et al. (69 authors), 2011b, ApJ, 736, 19
 Budding, E., 1984, A&A, 130, 324
 Budding, E., Demircan, O., 2007, *Introduction to Astronomical Photometry*, CUP
 Demircan, O., Eker, Z., Karataş, Y., Bilir, S., 2006, MNRAS, 366, 1511
 Devore, E., Koch, D., Gould, A., Harman, P., 2009, BAAS, 41, 412
 Erdem, A., Öztürk, O., 2014, MNRAS, 441, 1166
 Everett, M.E., Howell, S.B., Kinemuchi, K., 2012, PASP, 124, 316
 Esteves, L.J. De Mooij, E.J.W., Jayawardhana, R., 2013, ApJ, 772, 51
 Esteves, L.J. De Mooij, E.J.W., Jayawardhana, R., 2015, ApJ, 804, 150
 Hambleton K., et al. (10 authors), 2013, EAS, 64, 285
 Henrard J., 1982, Cel. Mech., 27, 3.
 Huber, D., et al. (34 authors), 2013, ApJ, 767, 127
 Johnson, J.A., et al. (9 authors) 2007, ApJ, 665, 785
 Kass, R.E., Raftery, A.E. 1995, J Amer Stat A, 90(430), 773
 Kipping, D.M., Spiegel, D.S., 2011, MNRAS, 417, 88
 Kopal, Z., 1959, *Close Binary Systems*, Chapman & Hall, London & New York
 Lillo-Box J. et al. (11 authors), 2014a, A&A, 562, A109
 Lillo-Box J. et al. (9 authors), 2014b, A&A, 568, L1
 Lin, D.N.C., Bodenheimer, P., Richardson, D.C., 1996, Nature, 380, 606
 Mandel, K., Agol, E., 2002, ApJ, 580, 171
 Muirhead, P.S., Hamren, K., Schlawin, E., Rojas-Ayala, B., Covey, K.R., Lloyd, J.P., 2012, ApJ, 750, 37
 Nagasawa, M., Ida, S., Bessho, T., 2008, ApJ, 678, 498
 Rhodes, M.D., 2015, WINKEPLER Manual, (version 2.16), <http://home.comcast.net/~michael.rhodes/>
 Rhodes, M.D., Budding, E., 2014, ApSS, 351,451
 Sato, B., et al. (9 authors) 2015, ApJ, 802, 57
 Schwarz, R., Dvorak, R., Süli, A., Erdi, B., 2007, AN, 328, 785
 Seager, S., Mallén-Ornelas, G., 2003, ApJ, 585, 1038.
 Shporer, A., Brown, T., Mazeh, T., Zucker, S., 2012, New A., 17, 309
 Sliski, D.H., Kipping, D.M., 2014, ApJ, 788, 148
 Souchay, J.J., Dvorak, R., 2010, *Dynamics of Small Solar System Bodies and Exoplanets*, Lecture Notes Phys., 790
 Szabó, R., Szabó, G.M., Dály, G., Simon A.E., Hodosán, G., Kiss, L.L., 2013, A&A, 553, A17
 Tenenbaum, P., et al. (30 authors), 2013, ApJS, 206, 5
 Villaver, E., Livio, M., 2009, ApJ, 785, L81
 Witte, M.G., Savonije, G.J., 1999, A&A, 350, 129
 Yoshida, F., Nakamura, T., 2005, AJ, 130, 2900
 Zahn J-P., 1977, A&A, 57, 383
 Zeilik, M., de Blasi, C., Rhodes, M., Budding, E., 1988, ApJ, 332, 293